Inorganic Chemistry

Article

pubs.acs.org/IC

Anion-Directed Assemblies of Cationic Metal–Organic Frameworks Based on 4,4′-Bis(1,2,4-triazole): Syntheses, Structures, Luminescent and Anion Exchange Properties

Xinxiong Li, Yaqiong Gong, Huaixia Zhao, and Ruihu Wang*

State Key Laboratory of Structural Chemistry, Fujian Institute of Research on the Structure of Matter, Chinese Academy of Sciences, Fuzhou, 350002, China

Supporting Information

ABSTRACT: Three cationic metal–organic frameworks (MOFs), $Ag(btr)\cdot PF_6\cdot 0.5CH_3CN$ (**1**), $Ag_2(btr)_2(H_2O)\cdot 2CF_3SO_3\cdot H_2O$ (**2**), and $Ag_2(btr)_2(NO_3)\cdot NO_3$ (**3**), were prepared from reaction of 4,4′-bis(1,2,4-triazole) (btr) with silver salts containing different anions. Complex **1** is a three-dimensional (3-D) framework constructed from tetrahedral-shaped nanoscale coordination cages with PF_6^- as counter-anions. **2** and **3** are 3-D architectures containing 1-D channels, in which charge-balancing $CF_3SO_3^-$ and NO_3^- are located in their respective channels. Luminescent emission of **1**–**3** shows an obvious red shift compared with the btr ligand. Anion exchange studies show that **1** is able to selectively exchange MnO_4^- in aqueous solution with a modest capacity of 0.56 mol mol^{-1}; the luminescent emission of **1** is quickly quenched upon MnO_4^- exchange.

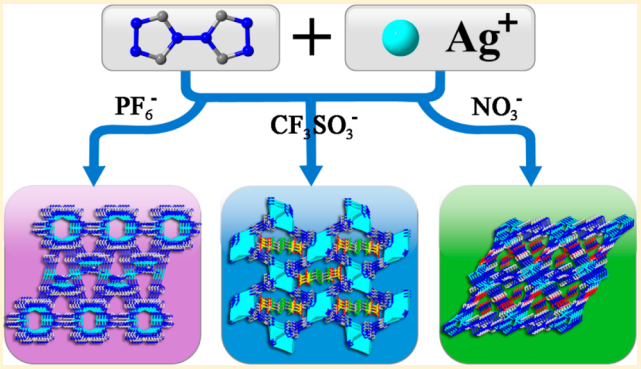

INTRODUCTION

The exploration of metal–organic frameworks (MOFs) has received tremendous attention because of their fascinating structures and widespread potential applications in gas adsorption/storage, chemical separation, catalysis, optical properties, and drug delivery.[1] A large number of MOFs with various structures and functions have been constructed by using metal ions/clusters as nodes and organic ligands as linkers.[2] Among various MOFs, cationic MOFs have distinct advantages in comparison with neutral MOFs in the design of functional materials. For example, cationic MOFs can serve as promising anion exchange materials through selective exchange of charge-balancing anions in the framework with other anions, leading to tunable change in physical properties.[3] Besides, cationic MOFs can serve as ionic hosts to accommodate different guest molecules by electrostatic interaction, which can cooperatively result in specific functions.[4] Hence, an increasing interest has recently shifted to the design and synthesis of cationic MOFs.[3−5]

As is well-known, the structures and performances of cationic MOFs have been influenced by several factors, such as organic ligands, metal ions, and charge-balancing anions.[6,7] In the construction of cationic MOFs, one of the most fruitful choices is taking advantage of neutral nitrogen-containing ligands that can bridge between transition-metal ions. Among a variety of neutral ligands, 4,4′-bis(1,2,4-triazole) (btr) is an attractive candidate. btr has four potential coordination nitrogen atoms, two triazoly rings may freely rotate through the N–N bond, which allows btr to exhibit bi-, tri-, and tetradentate bridging modes when coordinating with metal ions. Although a few btr-based cationic MOFs have been reported,[8−12] the difficulty of the exact prediction and control of final products is still one of the major challenges. Understanding the assembly process and bridging modes of btr is an important step to develop new functional materials.

Ag^+ is a good candidate in the preparation of MOFs owing to its strong coordination ability to nitrogen-donor atoms, and it also possesses various labile coordination geometries, such as linear, trigonal, tetrahedral, pentagonal, square-pyramidal, and even octahedral fashions. The assembly of Ag^+ with multi-dentate nitrogen-containing ligands produced various MOFs with intriguing structures and luminescent properties.[13] Very recently, we have reported a three-dimensional (3-D) cationic MOF consisting of two kinds of nanoscale coordination cages based on btr and Ag^+, which exhibits outstanding properties in capture, separation, and probe of dichromate in aqueous solution.[14] As a continuation of our efforts to explore cationic MOFs, herein, we report the syntheses and crystal structures of three unprecedented 3-D cationic MOFs, $Ag(btr)\cdot PF_6\cdot 0.5CH_3CN$ (**1**), $Ag_2(btr)_2(H_2O)\cdot 2CF_3SO_3\cdot H_2O$ (**2**), and $Ag_2(btr)_2(NO_3)\cdot NO_3$ (**3**). Complex **1** not only is able to selectively exchange MnO_4^- in aqueous solution but also can serve as a potential luminescent probe for MnO_4^-.

Received: August 14, 2014
Published: October 28, 2014

   dx.doi.org/10.1021/ic501978u | Inorg. Chem. 2014, 53, 12127−12134

Table 1. X-ray Crystallographic Data for 1−3

	1	2	3
empirical formula	$C_5H_{5.5}AgF_6N_{6.5}P$	$C_{10}H_{12}Ag_2F_6N_{12}O_8S_2$	$C_8H_8Ag_2N_{14}O_6$
formula weight	409.47	822.18	612.02
crystal system	tetragonal	monoclinic	monoclinic
space group	$I\bar{4}2d$	$P2_1/n$	$P2_1/n$
a (Å)	13.1338(4)	12.866(7)	9.153(3)
b (Å)	13.1338(4)	12.776(7)	17.895(5)
c (Å)	44.093(3)	16.802(9)	10.668(3)
α (deg)	90	90	90
β (deg)	90	105.303(10)	96.395(4)
γ (deg)	90	90	90
V (Å^3)	7605.9(5)	2664(2)	1736.5(8)
Z	24	4	4
F(000)	2808	1600	1184
ρ_{calcd} (g cm^{-3})	1.279	2.050	2.341
temp (K)	293	293	293
μ (mm^{-1})	1.554	1.728	2.323
refln. collected	22819	19904	14626
independent refln.	4264	5926	3956
parameters	151	371	271
GOF on F^2	1.098	1.011	1.118
final R indices ($I = 2\sigma(I)$)[a]	R_1 = 0.0666	R_1 = 0.0492	R_1 = 0.0480
	wR_2 = 0.2056	wR_2 = 0.1231	wR_2 = 0.0984
R indices (all data)[a]	R_1 = 0.0685	R_1 = 0.0662	R_1 = 0.0534
	wR_2 = 0.2091	wR_2 = 0.1377	wR_2 = 0.1019

[a] $R_1 = \sum||F_o| - |F_c||/\sum|F_o|$. $wR_2 = [\sum w(F_o^2 - F_c^2)^2/\sum w(F_o^2)^2]^{1/2}$; $w = 1/[\sigma^2(F_o^2) + (xP)^2 + yP]$, $P = (F_o^2 + 2F_c^2)/3$, where $x = 0.1600$, $y = 4.3344$ for **1**; $x = 0.0691$, $y = 0.3314$ for **2**; $x = 0.0294$, $y = 5.6040$ for **3**.

EXPERIMENTAL SECTION

Materials and General Methods. btr was synthesized according to the literature method;[15] other reagents were commercially available and used without further purification. Elemental analyses of C, H, and N were carried out with a Vario EL III elemental analyzer. Infrared (IR) spectra were recorded on an Opus Vertex 70 FT-IR infrared spectrophotometer in the range of 450−4000 cm^{-1}. Thermogravimatric analyses (TGA) were performed in a dynamic nitrogen atmosphere with a heating rate of 10 °C/min, using a NETZSCH STA449C thermal analyzer. Powder X-ray diffraction (PXRD) patterns were obtained using a Philips X'Pert-MPD diffractometer with Cu Kα radiation (λ = 1.54056 Å). Ultraviolet−visible (UV−vis) adsorption spectra were collected on a PerkinElmer Lambda 35 spectrophotometer. Luminescent spectra were recorded on an Edinburgh Instruments FLS920 spectrofluorimeter equipped with both continuous-wave (450 W) and pulse xenon lamps.

Synthesis of Ag(btr)·PF$_6$·0.5CH$_3$CN (1). An acetonitrile solution (10 mL) of $AgPF_6$ (0.40 mmol, 101 mg) was added to a stirring aqueous solution (10 mL) of btr (0.20 mmol, 27 mg) at room temperature. The resultant mixture was stirred for 30 min and then filtered. The filtrate was left standing in air for slow evaporation; colorless block crystals suitable for X-ray diffraction were obtained after 3 days. Yield: 75 mg (90%, based on btr). Elemental analysis (%) calcd for $C_4H_4N_6PF_6Ag{\cdot}0.5CH_3CN$: C 14.66, H 1.35, N 22.23; found: C 14.98, H 1.53, N 22.79. IR (KBr, cm^{-1}): 3655(w), 3147(s), 2952(w), 2269(w), 1712(w), 1510(s), 1301(m), 1085(vs), 1009(s), 827(vs), 614(vs), 557(vs).

Syntheses of Ag$_2$(btr)$_2$(H$_2$O)·2CF$_3$SO$_3$·H$_2$O (2). 2 was prepared based on the procedures similar to that of **1** except for the replacement of $AgPF_6$ by $AgCF_3SO_3$ (0.40 mmol, 103 mg). Yield: 25 mg (30%, based on btr). Elemental analysis (%) calcd for $C_8H_{10}N_{12}OAg_2{\cdot}2CF_3SO_3{\cdot}H_2O$: C 14.61, H 1.47, N 20.44, S 7.80; found: C 14.51, H 1.80, N 20.44, S 7.79. IR (KBr, cm^{-1}): 3447(m), 3147(s), 3098(s), 1636(w), 1450(s), 1263(vs), 1162(vs), 1075(s), 1036(vs), 982(m), 926(m), 862(m), 758(m), 646(vs), 611(vs), 575(w), 519(m).

Syntheses of Ag$_2$(btr)$_2$(NO$_3$)·NO$_3$ (3). 3 was prepared based on the procedures similar to that of **1** except for the replacement of $AgPF_6$ by $AgNO_3$ (0.40 mmol, 68 mg) in 20 mL of acetonitrile. Yield: 47 mg (76%, based on btr). Elemental analysis (%) calcd for $C_8H_8N_{13}O_3Ag_2{\cdot}NO_3$: C 15.70, H 1.32, N 32.04; found: C 15.78, H 1.26, N 32.11. IR (KBr, cm^{-1}): 3447(m), 3146(s), 3101(s), 3017(m), 1763(w), 1698(m), 1379(vs), 1295(m), 1228(w), 1199(w), 1088(s), 1059(s), 1015(w), 982(m), 924(m), 885(m), 827(m), 612(vs).

Anion Exchange of MnO$_4^-$ in Complex 1. As-synthesized **1** (41 mg, 0.10 mmol) was immersed in an aqueous solution (20 mL) of $KMnO_4$ (0.0050 mol·L^{-1}, 0.10 mmol MnO_4^-), and the mixture was shaken at room temperature for 24 h. The anion exchange process was monitored by liquid UV−vis spectroscopy based on typical absorption of MnO_4^- at 525 nm. A 0.1 mL aliquot of the aqueous $KMnO_4$ solution was pipetted at different time intervals and was diluted using 2 mL of deionized water to measure the UV−vis adsorption intensity. The anion exchange capacity of **1** was evaluated by measuring the decolorization rate of the aqueous $KMnO_4$ solution, which was calculated by the following formula

$$D = \frac{C_0 - C_1}{C_0} \times 100\% = \frac{A_0 - A_1}{A_0} \times 100\%$$

where D is adsorption capacity, and C_0, A_0 and C_1, A_1 are the concentration and absorbency of the aqueous $KMnO_4$ solution at the peak of 525 nm before and after anion exchange, respectively.

Selective Anion Exchange in Complex 1. As-synthesized **1** (41 mg, 0.10 mmol) was immersed in an aqueous solution (20 mL) of $KMnO_4$ (0.0050 mol·L^{-1}, 0.10 mmol MnO_4^-), KNO_3 (10 mg, 0.10 mmol), $NaBF_4$ (11 mg, 0.10 mmol), and $NaClO_4$ (14 mg, 0.10 mmol). After the mixture was shaken at room temperature for 2 h, the resultant crystals were filtered, rinsed with deionized water, dried in air, and used for XRD and IR analyses.

Selective Anion Exchange with Trace Amount of MnO$_4^-$. As-synthesized **1** (41 mg, 0.10 mmol) was immersed in an aqueous solution (0.2 mL) of $KMnO_4$ (0.0050 mol·L^{-1}, 0.0010 mmol MnO_4^-), KNO_3 (10 mg, 0.10 mmol), $NaBF_4$ (11 mg, 0.10 mmol), and $NaClO_4$

dx.doi.org/10.1021/ic501978u | Inorg. Chem. 2014, 53, 12127−12134

(14 mg, 0.10 mmol). After the mixture was shaken at room temperature for 2 h, the resultant crystals were filtered, rinsed with deionized water, dried in air, and used for XRD and IR analyses.

X-ray Crystallography. Single-crystal X-ray diffraction data for **1**–**3** were collected on a Rigaku MM007-CCD diffractometer with graphite-monochromated Mo Kα (λ = 0.71073 Å) at room temperature. The program SADABS was used for the absorption correction. The structure was solved by a direct method and refined on F^2 by full-matrix least-squares methods using the SHELX-97 program package.[16] All non-hydrogen atoms were refined anisotropically. The hydrogen atoms of btr and water molecules were generated geometrically. In **1**, the charge-balancing anions and solvent molecules cannot be mapped due to the high symmetry of the framework structure, which are often observed in MOFs.[17] The residual electron density that could not sensibly be modeled as solvent or anions were removed via application of the SQUEEZE function of PLATON. The final formula of **1** was determined by combining the results of the elemental analysis with thermogravimetric analysis. Crystallographic data and structural refinement for **1**–**3** are summarized in Table 1. CCDC: 982558–982560.

RESULTS AND DISCUSSION

Synthesis. It is well-known that the type, size, shape and geometry of anions play important roles in the construction of cationic MOFs. The anions not only can coordinate to metal centers in a monodentate or multidentate modes but also can serve as templates in the assembly process of organic ligands and metal ions, resulting in various MOFs with different structures and functions. When tetrahedral-shaped ClO_4^- was used as a counteranion, the reaction of btr with Ag^+ afforded a 3-D cationic MOF consisting of two types of coordination cages;[14] its novel structure and promising application in capture and recognition of dichromate encouraged us to further explore the cationic frameworks based on btr and Ag^+ with other anions. The replacement of ClO_4^- with octahedral-shaped PF_6^- generated a quite different 3-D cationic MOF consisting of tetrahedral cages. The use of antitrigonal prism-shaped and large-sized $CF_3SO_3^-$ led to the formation of a unique 3-D cationic MOF containing 1-D channels. It should be mentioned that PF_6^- in complex **1** and $CF_3SO_3^-$ in complex **2** are not involved in coordinating; they just serve as counteranions of cationic MOFs to balance charge. However, when trigonal-shaped NO_3^- was used as a counteranion under the same conditions, a completely different 3-D cationic MOF was obtained. NO_3^- in complex **3** not only balances charge in the cationic framework but also takes part in coordinating with Ag^+. These results show that anions have important effects on the self-assembly process of btr and Ag^+, which results in different bridging modes of btr and cationic MOFs with different structures.

Structural Description of Ag(btr)·PF_6·0.5CH_3CN (1). Single-crystal X-ray diffraction analysis has revealed that **1** crystallizes in the noncentrosymmetric tetragonal space group $I\bar{4}2d$ and exhibits a 3-D structure consisting of tetrahedral-shaped coordination cages. As shown in Figure 1, two crystallographically independent Ag^+ ions adopt a distorted tetrahedral geometry and are coordinated by four nitrogen atoms from different btr ligands. Two independent Ag^+ ions (Ag1 and Ag2) are connected by four nitrogen atoms (N5, N6, N8, and N9) to form a binuclear six-membered Ag_2N_4 metallacycle (Figure 1), in which the distance of Ag1 and Ag2 is 3.545(5) Å. Two crystallographically independent btr ligands act as a μ_4-bridge (Scheme 1a), and the dihedral angels between two triazolyl rings are 77.766(3)° and 80.018(2)°, respectively. The most intriguing structural feature in **1** is the

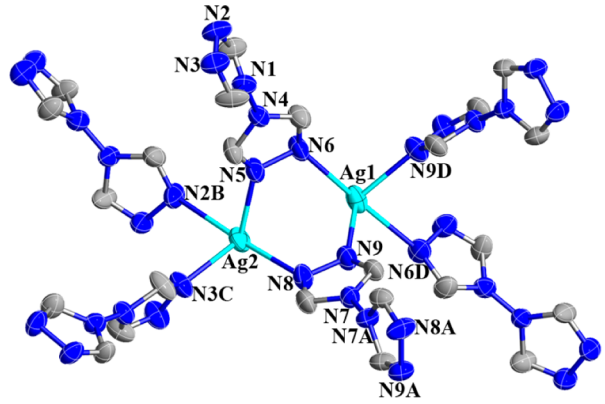

Figure 1. View of coordination environments of Ag^+ ions in **1** with thermal ellipsoids at 50% level. Symmetry codes: A: 1 − *x*, −*y*, *z*; B: −0.5 + *x*, 0.5 − *y*, 0.5 − *z*; C: 0.5 − *x*, −0.5 + *y*, 0.5 − *z*; D: *x*, 0.5 − *y*, 0.25 − *z*.

Scheme 1. Coordination Modes of btr in 1–3

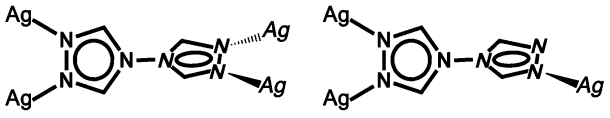

existence of distorted tetrahedral coordination cages. Every tetrahedral cage is composed of four Ag^+ as nodes and six btr ligands as linkers (Figure 2a,b). The overall edge length is about 1.3 nm, and the aperture of the trigonal windows is about 3.5 Å. Worthy of mention is the further assembly of these tetrahedral nanoscale cages. Each cage is connected to four neighboring ones by sharing Ag_2N_4 metallacycles (Figure 2c), which is further linked by another four cages through four Ag^+ (Figure 2d; Figure S1, Supporting Information). In other words, each cage can be viewed as an eight-connected node and is interconnected with eight neighboring cages (Figure 2e; Figure S2, Supporting Information) to generate a 3-D cationic framework (Figure 3). Although a large number of cationic MOFs have been reported,[18] cationic MOFs constructed from nanoscale coordination cages are relatively rare.[19] The 3-D framework possesses three kinds of channels along the *a* axis, including a hexagonal channel (A) and irregular channels (B and C). The diameters of these channels are about 5.4, 4.9, and 4.2 Å for A, B, and C, respectively, which are large enough for anion exchange. PLATON calculation shows that the total empty volume of the cationic framework is 3820 Å^3, corresponding to 50.2% of the total crystal volume (7606 Å^3). The cavities and channels of **1** are filled with disordered PF_6^- and solvent molecules that cannot be mapped by single-crystal X-ray diffraction, which is often observed in MOFs.[17]

Structural Description of Ag_2(btr)$_2$(H_2O)·2CF_3SO_3·H_2O (2). Complex **2** is a 3-D framework containing 1-D channels; its asymmetric unit contains two Ag^+ ions, two btr ligands, one coordinated water, two $CF_3SO_3^-$ anions, and one lattice water molecule. As depicted in Figure 4, all Ag^+ ions are in a distorted tetrahedral geometry, where Ag1 is coordinated by four nitrogen atoms from different btr ligands, while Ag2 is coordinated by three nitrogen atoms from different btr ligands and one water molecule. The Ag–N bond distances range from 2.182(4) to 2.410(4) Å, which are shorter than the Ag–O bond length of 2.719(2) Å. Different from **1**, two crystallographically

dx.doi.org/10.1021/ic501978u | *Inorg. Chem.* 2014, 53, 12127–12134

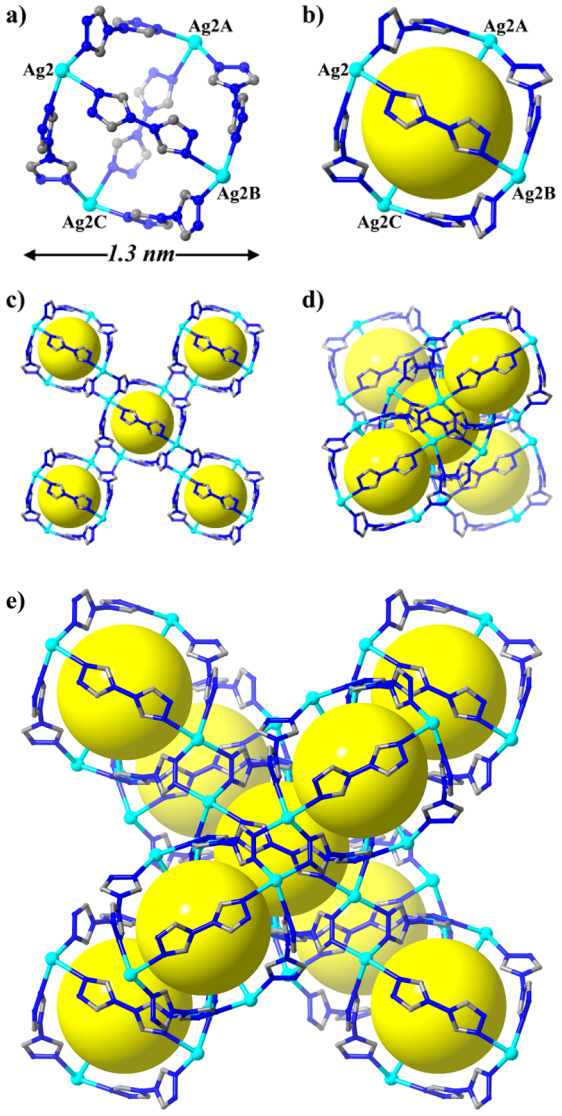

Figure 2. (a, b) Ball-and-stick representation of tetrahedral cage in **1**. (c) View of the connection mode of one cage with four neighboring ones by sharing Ag_2N_4 metallacycles. (d) View of the connection mode of one cage with another four neighboring ones through Ag^+ ions. (e) View of final connection mode of one cage with eight neighboring ones.

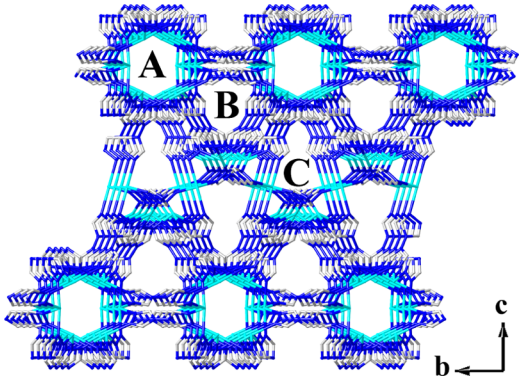

Figure 3. View of the 3-D cationic framework in **1**, showing three kinds of channels along the *a* axis.

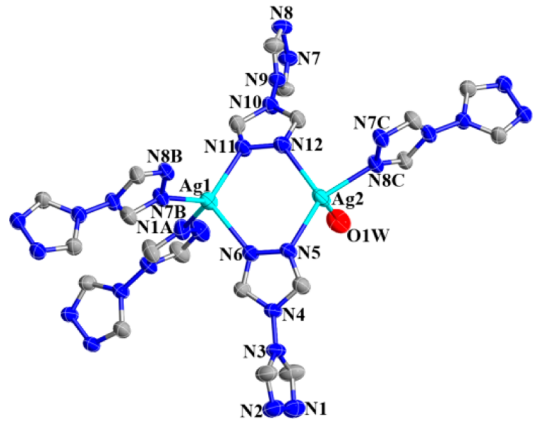

Figure 4. View of coordination environments of Ag^+ ions in **2** with thermal ellipsoids at 50% level. Symmetry codes: A: 0.5 − *x*, 0.5 + *y*, −2.5 − *z*; B: −0.5 + *x*, −0.5 − *y*, −0.5 + *z*; C: −0.5 − *x*, 0.5 + *y*, −1.5 − *z*.

independent btr ligands show different bridging modes. One acts as a μ_4-bridge connecting four Ag^+ ions (Scheme 1a), which is similar to that in **1**. The other serves as a μ_3-bridge binding to three Ag^+ ions (Scheme 1b). In complex **2**, the μ_4-btr ligand connects Ag^+ ions to form a 2-D layer with 28-membered macrocycles (Figure 5), which is further linked by

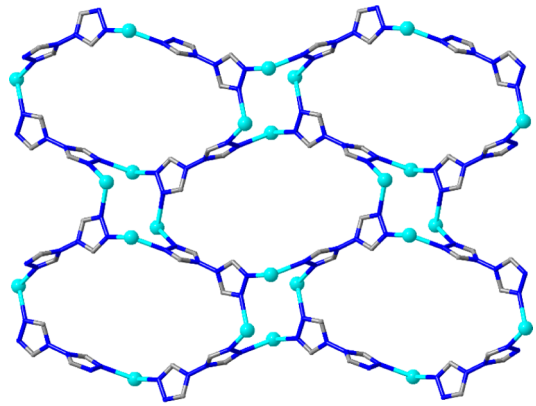

Figure 5. View of the 2-D layer constructed from Ag^+ ions and μ_4-btr in **2**.

μ_3-btr to give rise to an unusual 3-D cationic framework (Figure 6). The most intriguing structure point in **2** is that the framework possesses a 1-D channel along the *a* axis with a diameter of about 6.9 Å, in which $CF_3SO_3^-$ anions and lattice water molecules are located. After removal of charge-balancing anions and water molecules, the total potential accessible volume in the cationic framework is 48.0% based on PLATON calculation, which is slightly smaller than that in complex **1**.

Structural Description of $Ag_2(btr)_2(NO_3)\cdot NO_3$ (3). X-ray structure analysis reveals that **3** crystallizes in the monoclinic space group $P2_1/n$ and presents a 3-D structure. In the asymmetric unit of **3**, there are two Ag^+ ions, two btr ligands, and two NO_3^- anions. As illustrated in Figure 7, Ag^+ ions have a distorted tetrahedral geometry, where Ag1 is coordinated by three nitrogen atoms from different btr ligands and one oxygen atom of NO_3^-, while Ag2 is connected by four nitrogen atoms from different btr ligands. The Ag−N bond distances fall in the range from 2.196(4) to 2.619(4) Å, which is shorter than the Ag−O bond length of 2.650(1) Å. Similar to **2**, there are two

dx.doi.org/10.1021/ic501978u | *Inorg. Chem.* 2014, 53, 12127−12134

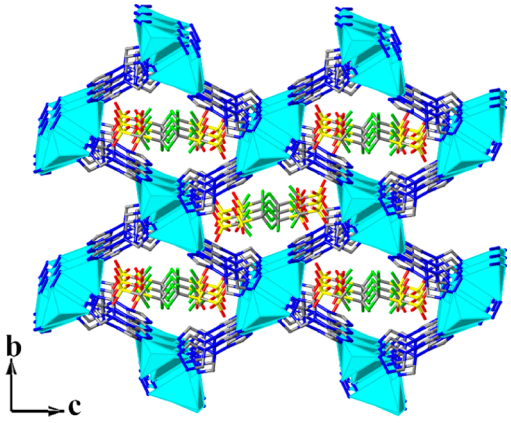

Figure 6. View of the 3-D framework along the *a* axis in **2**. Green: F, yellow: S.

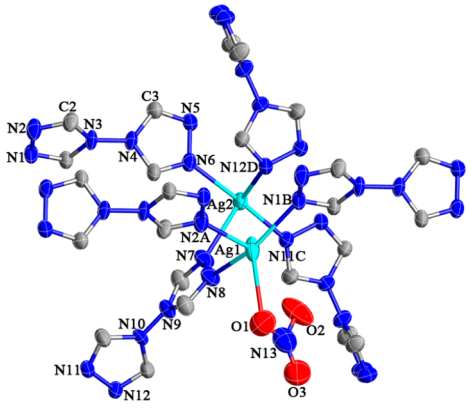

Figure 7. View of coordination environments of Ag^+ ions in complex **3** with thermal ellipsoids at 50% level. Symmetry codes: A: $1 - x$, $1 - y$, $1 - z$; B: x, y, $1 + z$; C: $0.5 + x$, $0.5 - y$, $0.5 + z$; D: $1.5 - x$, $0.5 + y$, $1.5 - z$.

kinds of btr ligands with μ_3- and μ_4-bridging modes, respectively (Scheme 1). The dihedral angles between two triazoyl rings in μ_3-btr and μ_4-btr are 59.528(2)° and 78.805°, respectively. In complex **3**, Ag^+ ions are connected by μ_4-btr to form a 2-D layer (Figure 8), which is further linked by μ_3-btr to generate a 3-D network with 1-D channels along the *c* axis (Figure 9). The uncoordinated NO_3^- occupies the channels to balance the charge. The total potential accessible volume of the

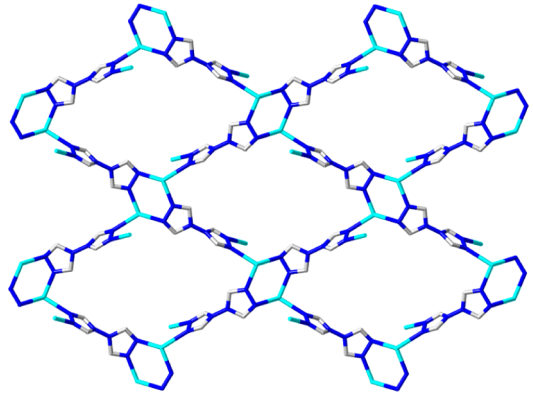

Figure 8. View of the 2-D layer constructed from Ag^+ ions and μ_4-btr ligands in **3**.

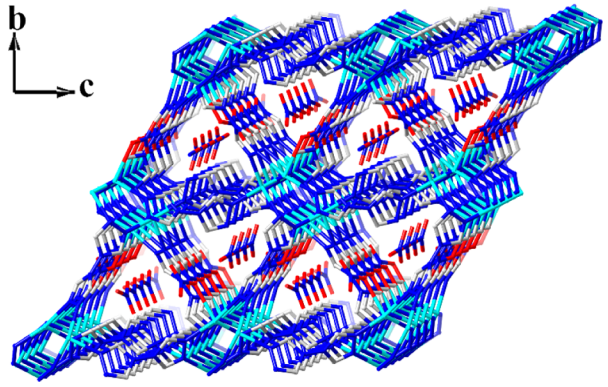

Figure 9. View of the 3-D framework along the *a* axis in **3**.

cationic framework is estimated by the PLATON program and is about 11.7% of the total crystal volume after the removal of uncoordinated NO_3^-, which is much lower than that of **1** and **2**.

PXRD, IR, and TGA Characterization. In the PXRD patterns of **1**−**3** (Figures S3−S5, Supporting Information), the good accordance between the experimental patterns and the simulated ones indicates good phase purities. The IR spectra of **1**−**3** are shown in Figures S6−S8 (Supporting Information). Characteristic vibration bands of PF_6^-, $CF_3SO_3^-$, and NO_3^- were observed at 831, 1263, and 1385 cm^{-1},[20] respectively, which are consistent with their single-crystal structural analysis. TGA curves of **1**−**3** are shown in Figure S9 (Supporting Information). For **1**, a weight loss of 4.76% in the range of 30−90 °C was observed, corresponding to the removal of acetonitrile guest molecules (calcd: 5.01%). There is no obvious weight loss before the framework starts to decompose at 270 °C. For **2**, the weight loss from 30 to 150 °C is 2.39%, which is assigned to the release of one lattice water molecule (calcd: 2.19%); no obvious weight loss occurs before 280 °C. However, the cationic framework in **3** is stable up to 230 °C and then begins to break down drastically due to high nitrogen content and good oxygen balance, which is common in energetic MOFs.[21]

Luminescent Properties. The photoluminescence properties of the btr ligand and complexes **1**−**3** were investigated in the solid state at room temperature. Upon excitation at 345 nm, the free btr ligand displays a strong emission with a maximum around 420 nm (Figure 10), which is assigned to $\pi \rightarrow \pi^*$

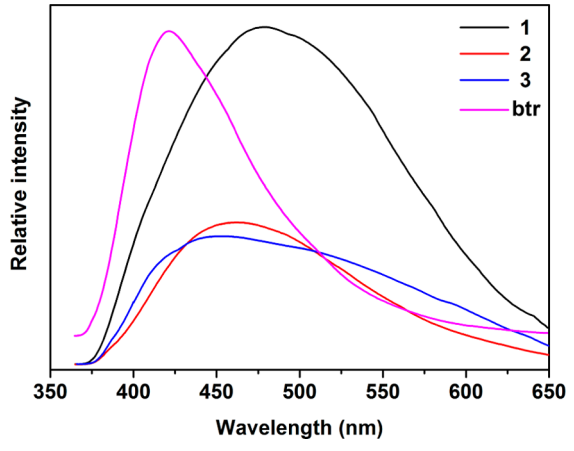

Figure 10. Room-temperature solid-state emission spectra of btr and complexes **1**−**3**.

dx.doi.org/10.1021/ic501978u | *Inorg. Chem.* 2014, 53, 12127−12134

transitions. However, the strongest emissions occur at 478 nm for **1**, 461 nm for **2**, and 445 nm for **3** upon excitation at 345 nm, respectively (Figure 10), showing a significant red shift compared with the free btr ligand. The emissions of complexes **1**−**3** can be attributed to the ligand-to-metal charge transfer.[22] The different coordination behaviors of btr and different counteranions in the framework are probably responsible for the shift difference of the emission bands in **1**−**3**.

Anion Exchange Property. Given the cationic framework of complex **1** with three kinds of channels and PF_6^- located in the void, the monovalent MnO_4^- was chosen as a model to investigate the anion exchange property of **1**. The exchange process was monitored by UV−vis spectroscopy at intervals based on the variation of the maximum adsorption peak of MnO_4^- at 525 nm.[23] As shown in Figure 11, when crystals of **1**

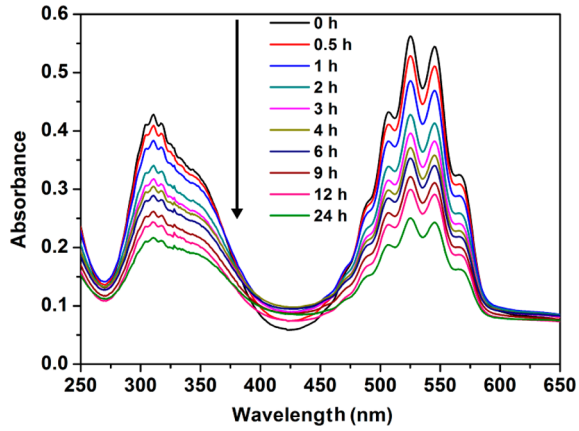

Figure 11. UV−vis spectra of aqueous $KMnO_4$ solution during anion exchange with equimolar **1**.

were immersed in a 20 mL aqueous solution containing equimolar $KMnO_4$, the MnO_4^- concentration in the solution decreased by 14% and 24% after 1 and 2 h, respectively, corresponding to the exchange capacities of 0.14 and 0.24 mol mol^{-1}, respectively. Subsequently, the MnO_4^- concentration was slowly decreased. The overall exchange capacity of MnO_4^- in 24 h is 0.56 mol mol^{-1}. Simultaneously, the color of the crystals changed from colorless to deep purple (Figure 12b), implying the existence of MnO_4^- in the solid. After anion exchange, the sample of **1** was filtrated, rinsed with water, and

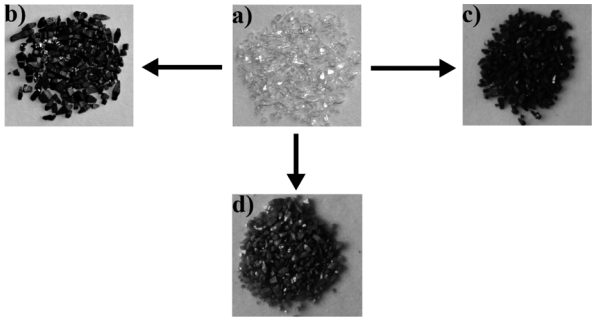

Figure 12. Color of (a) as-synthesized **1**; (b) 0.10 mmol of **1** immersed in a 20 mL aqueous solution containing equimolar $KMnO_4$ for 24 h; (c) 0.10 mmol of **1** immersed in a 20 mL aqueous solution containing equimolar $KMnO_4$, KNO_3, $NaBF_4$ and $NaClO_4$ for 2 h; (d) 0.10 mmol of **1** immersed in a 20 mL of aqueous solution containing equimolar KNO_3, $NaBF_4$, $NaClO_4$ and 0.001 mmol of $KMnO_4$ for 2 h.

dried in air. In the IR spectra (Figure 13b), the emergence of the characteristic adsorption band of MnO_4^- at 888 cm^{-1}[23,24]

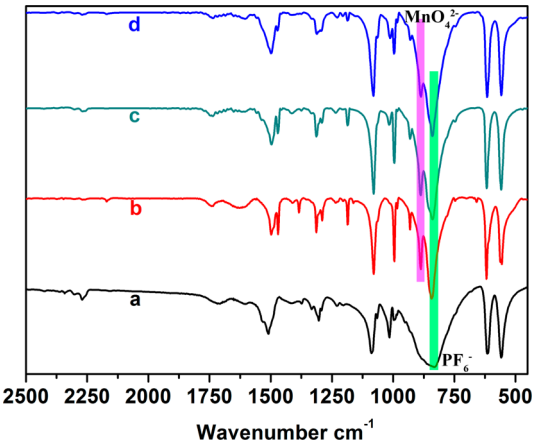

Figure 13. IR spectra for (a) as-synthesized **1**; (b) 0.10 mmol of **1** immersed in a 20 mL aqueous solution containing equimolar $KMnO_4$ for 24 h; (c) 0.10 mmol of **1** immersed in a 20 mL aqueous solution containing equimolar $KMnO_4$, KNO_3, $NaBF_4$ and $NaClO_4$ for 2 h; (d) 0.10 mmol of **1** immersed in a 20 mL aqueous solution containing equimolar KNO_3, $NaBF_4$ and $NaClO_4$ and 0.001 mmol of $KMnO_4$ for 2 h.

and the concomitant decrement of the broad band of PF_6^- at 831 cm^{-1}[20] indicate that MnO_4^- enters the cationic framework of **1** by exchanging with PF_6^-. XRD measurements indicate that the 3-D cationic framework remained intact during the anion exchange (Figure 14), suggesting good stability of the cationic framework.

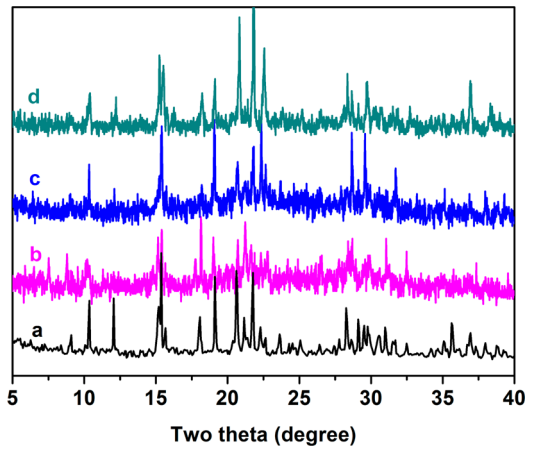

Figure 14. XRD patterns for (a) as-synthesized **1**; (b) 0.10 mmol of **1** immersed in a 20 mL aqueous solution containing equimolar $KMnO_4$ for 24 h; (c) 0.10 mmol of **1** immersed in a 20 mL aqueous solution containing equimolar $KMnO_4$, KNO_3, $NaBF_4$ and $NaClO_4$ for 2 h; (d) 0.10 mmol of **1** immersed in a 20 mL aqueous solution containing equimolar KNO_3, $NaBF_4$, $NaClO_4$ and 0.001 mmol $KMnO_4$ for 2 h.

Anion selectivity was also examined. When crystals of **1** were immersed in a 20 mL aqueous solution containing equimolar $KMnO_4$, KNO_3, $NaBF_4$ and $NaClO_4$ for 2 h, the crystal color turned to deep purple (Figure 12c). In the IR spectra (Figure 13c), no obvious characteristic bands of NO_3^-, BF_4^-, and ClO_4^- were observed, and an obvious characteristic band of MnO_4^- was found, indicating good selectivity of MnO_4^- over

dx.doi.org/10.1021/ic501978u | Inorg. Chem. 2014, 53, 12127−12134

NO_3^-, BF_4^-, and ClO_4^-. To further demonstrate selectivity of the framework in exchanging MnO_4^-, a similar experiment was also carried out under a low concentration of $KMnO_4$. Interestingly, when the amount of MnO_4^- was decreased to 1/100 compared with NO_3^-, BF_4^- and ClO_4^-, **1** still can selectively exchange MnO_4^-, as proved by the color change of the crystals (Figure 12d) and the appearance of the characteristic peak of MnO_4^- in IR spectra (Figure 13d).

The effects of anion exchange on luminescent properties were also explored. As shown in Figure 15, the intensity of the luminescent emission in **1** dropped rapidly after the exchange of PF_6^- by MnO_4^-. The rapid disappearance of the luminescent emission after anion exchange for 0.5 h is probably attributed that the electron-transfer transitions of MnO_4^- decrease the energy transfer from btr to Ag^+.[25] As a result, **1** may be considered as a potential luminescent probe for MnO_4^-.

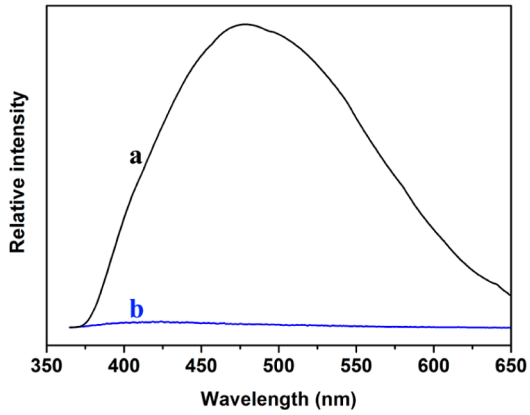

Figure 15. Room-temperature solid-state emission spectra upon excitation at 350 nm for (a) as-synthesized **1**; (b) 0.10 mmol of **1** immersed in a 20 mL aqueous solution containing equimolar $KMnO_4$ for 0.5 h.

CONCLUSIONS

Three 3-D cationic MOFs have been successfully prepared by the reactions of 4,4′-bis(1,2,4-triazole) with Ag^+ ions containing different counteranions. The type, size, and shape of anions have important effects on bridging modes of btr and the cationic frameworks of final products. btr in complex **1** serves as a μ_4-bridge, while btr in **2** and **3** exhibits μ_4- and μ_3-bridging fashions despite that Ag^+ in **1**−**3** adopts a distorted tetrahedral geometry. Luminescent emissions of **1**−**3** show different red shifts compared with that of the free btr ligand. Anion exchange investigations indicate that **1** can selectively exchange MnO_4^- in aqueous solution, and the luminescent emission of **1** is quickly quenched upon MnO_4^- exchange. In summary, this work not only enriches the structural diversity of cationic MOFs but also may provide a feasible strategy for constructing cationic MOFs with fascinating structures and desirable properties.

ASSOCIATED CONTENT

Supporting Information

Crystallographic data for **1**−**3** in CIF format, additional structural figures, PXRD patterns, IR spectra, and TGA curves for complexes **1**−**3**. This material is available free of charge via the Internet at http://pubs.acs.org.

AUTHOR INFORMATION

Corresponding Author

*E-mail: ruihu@fjirsm.ac.cn (R.W.).

Notes

The authors declare no competing financial interest.

ACKNOWLEDGMENTS

The authors acknowledge the 973 Program (2010CB933501, 2011CBA00502) and the National Natural Science Foundation of China (21273239, 21401195) for financial support.

REFERENCES

(1) (a) Murray, L. J.; Dinca, M.; Long, J. R. *Chem. Soc. Rev.* **2009**, *38*, 1294−1314. (b) Suvendu, S. M.; Asamanjoy, B.; Alexandra, K.; Uwe, S.; Christoph, J.; Hans-Jürgen, H. *J. Am. Chem. Soc.* **2014**, *136*, 44−47. (c) Tian, D.; Chen, Q.; Bu, X. H. *Angew. Chem., Int. Ed.* **2014**, *53*, 837−841. (d) Chaemchuen, S.; Verpoort, F. *Chem. Soc. Rev.* **2013**, *42*, 9304−9332. (e) Li, J. R.; Sculley, J.; Zhou, H. C. *Chem. Rev.* **2012**, *112*, 869−932.

(2) (a) Stock, N.; Biswas, S. *Chem. Rev.* **2011**, *112*, 933−969. (b) Ouellette, W.; Jones, S.; Zubieta, J. *CrystEngComm* **2011**, *13*, 4457−4485. (c) Qiu, S.; Zhu, G. *Coord. Chem. Rev.* **2009**, *253*, 2891−2911.

(3) (a) Cui, Y.; Xu, H.; Yue, Y.; Guo, Z.; Yu, J.; Chen, Z.; Gao, J.; Yang, Y.; Qian, G.; Chen, B. *J. Am. Chem. Soc.* **2012**, *134*, 3979−3982. (b) Wang, C.; Lin, W. *J. Am. Chem. Soc.* **2011**, *133*, 4232−4235.

(4) (a) Chakrabarty, R.; Mukherjee, P. S.; Stang, P. J. *Chem. Rev.* **2011**, *111*, 6810−6918. (b) Fei, H. H.; Oliver, S. R. J. *Dalton Trans.* **2010**, *39*, 11193−11120. (c) Xin, B. X.; Zeng, G.; Gao, L.; Li, Y.; Xing, S. H.; Hua, J.; Li, G. H.; Shi, Z.; Feng, S. H. *Dalton Trans.* **2013**, *42*, 7562−7568. (d) Han, Y.; Li, J. R.; Xie, Y. B.; Guo, G. S. *Chem. Soc. Rev.* **2014**, *43*, 5952−5981. (e) Mao, C. Y.; Kudla, R. A.; Zuo, F.; Zhao, X.; Mueller, L. J.; Bu, X. H.; Feng, P. Y. *J. Am. Chem. Soc.* **2014**, *136*, 7579−7582.

(5) Padial, N. M.; Quartapelle Procopio, E.; Montoro, C.; López, E.; Oltra, J. E.; Colombo, V.; Maspero, A.; Masciocchi, N.; Galli, S.; Senkovska, I.; Kaskel, S.; Barea, E.; Navarro, J. A. R. *Angew. Chem., Int. Ed.* **2013**, *52*, 8290−8294.

(6) (a) Li, Z.; Li, M.; Zhou, X. P.; Wu, T.; Li, D.; Ng, S. W. *Cryst. Growth Des.* **2007**, *7*, 1992−1998. (b) Bao, S. S.; Ma, L. F.; Wang, Y.; Fang, L.; Zhu, C. J.; Li, Y. Z.; Zheng, L. M. *Chem.—Eur. J.* **2007**, *13*, 2333−2343. (c) Dvoyashkin, M.; Valiullin, R.; Kärger, J.; Einicke, W. D.; Gläser, R. *J. Am. Chem. Soc.* **2007**, *129*, 10344−10345. (d) Kleij, A. W.; Kuil, M.; Tooke, D. M.; Spek, A. L.; Reek, J. N. H. *Inorg. Chem.* **2007**, *46*, 5829−5831.

(7) (a) Notash, B.; Safari, N.; Khavasi, H. R. *Inorg. Chem.* **2010**, *49*, 11415−11420. (b) Gulbransen, J. L.; Fitchett, C. M. *CrystEngComm* **2012**, *14*, 5394−5397. (c) Mastropietro, T. F.; Marino, N.; Armentano, D.; De Munno, G.; Yuste, C.; Lloret, F.; Julve, M. *Cryst. Growth Des.* **2013**, *13* (1), 270−281. (d) Mitra, A.; Hubley, C. T.; Panda, D. K.; Clark, R. J.; Saha, S. *Chem. Commun.* **2013**, *49*, 6629−6631. (e) Wang, D. X.; Fa, S. X.; Liu, Y.; Hou, B. Y.; Wang, M. X. *Chem. Commun.* **2012**, *48*, 11458−11460. (f) Chen, J.; Wang, S. H.; Liu, Z. F.; Wu, M. F.; Xiao, Y.; Zheng, F. K.; Guo, G. C.; Huang, J. S. *New J. Chem.* **2014**, *38* (1), 269−276.

(8) (a) Zilverentant, C. L.; Driessen, W. L.; Haasnoot, J. G.; Kolnaar, J. J. A.; Reedijk, J. *Inorg. Chim. Acta* **1998**, *282*, 257−260. (b) Zhang, X. C.; Chen, Y. H.; Liu, B. *Inorg. Chem. Commun.* **2008**, *11*, 446−449. (c) Huang, Y. Q.; Zhao, X. Q.; Shi, W.; Liu, W. Y.; Chen, Z. L.; Cheng, P. *Cryst. Growth Des.* **2008**, *8*, 3652−3660. (d) Lysenko, A. B.; Govor, E. V.; Krautscheid, H.; Domasevitch, K. V. *Dalton Trans.* **2006**, 3772−3776.

(9) Govor, E. V.; Lysenko, A. B.; Rusanov, E. B.; Domasevitch, K. V. *Z. Anorg. Allg. Chem.* **2010**, *636*, 209−217.

(10) (a) Andrzej, O.; Yu, S. Z.; Bruce, R. M. *Inorg. Chem.* **1991**, *30*, 3167−3174. (b) Yann, G.; Oliver, K.; Louis, R.; Benoit, C. *Inorg. Chem.* **1999**, *38*, 4663−4670.

(11) Wang, X. Y.; Wang, L.; Wang, Z. M.; Su, G.; Gao, S. *Chem. Mater.* **2005**, *17*, 6369−6380.
(12) (a) Lysenko, A. B.; Govor, E. V.; Domasevitch, K. V. *Inorg. Chim. Acta* **2007**, *360*, 55−60. (b) Vincent, L.; Sébastien, P.; Chiara, C.; Mohamed, S.; Jean-François, L.; Philippe, G.; Claude, L. *Eur. J. Inorg. Chem.* **2007**, 5693−5706.
(13) (a) Wu, J. C.; Zhao, L.; Wang, D. X.; Wang, M. X. *Inorg. Chem.* **2012**, *5*, 3860−3867. (b) Hu, W. J.; Liu, L. Q.; Ma, M. L.; Zhao, X. L.; Liu, Y. A.; Mi, X. Q.; Jiang, B.; Wen, K. *Inorg. Chem.* **2013**, *52*, 9309−9319.
(14) Li, X. X.; Xu, H. Y.; Kong, F. Z.; Wang, R. H. *Angew. Chem., Int. Ed.* **2013**, *52*, 13769−13773.
(15) Naik, A. D.; Marchand-Brynaert, J.; Garcia, Y. *Synthesis* **2008**, *1*, 149−154.
(16) (a) Sheldrick, G. M. *SHELXS97: Program for Crystal Structure Solution*; University of Göttingen: Göttingen, Germany, 1997. (b) Sheldrick, G. M. *SHELXL97: Program for Crystal Structure Refinement*; University of Göttingen: Göttingen, Germany, 1997.
(17) (a) Zheng, S. T.; Zuo, F.; Wu, T.; Feng, P. Y.; Bu, X. H. *Angew. Chem., Int. Ed.* **2011**, *50*, 1849−1852. (b) Kang, Y.; Wang, F.; Zhang, J.; Bu, X. H. *J. Am. Chem. Soc.* **2012**, *134*, 17881−17884.
(18) (a) Oliver, S. R. J. *Chem. Soc. Rev.* **2009**, *38*, 1868−1881. (b) Liu, S. X.; Xie, L. H.; Gao, B.; Zhang, C. D.; Sun, C. Y.; Li, D. H.; Su, Z. M. *Chem. Commun.* **2005**, 5023−5025. (c) Fei, H. H.; Rogow, D. L.; Oliver, S. R. J. *J. Am. Chem. Soc.* **2010**, *132*, 7202−7209. (d) Chen, X. D.; Wan, C. Q.; Sung, H. H. Y.; Williams, I. D.; Mak, T. C. W. *Chem.—Eur. J.* **2009**, *15*, 6518−6528. (e) Nickerl, G.; Notzon, A.; Heitbaum, M.; Senkovska, I.; Glorius, F.; Kaskel, S. *Cryst. Growth Des.* **2013**, *13*, 198−203.
(19) (a) Liu, D.; Li, H. X.; Ren, Z. G.; Chen, Y.; Zhang, Y.; Lang, J. P. *Cryst. Growth Des.* **2009**, *9*, 4562−4566. (b) Xue, Z. Z.; Sheng, T. L.; Zhu, Q. L.; Yuan, D. Q.; Wang, Y. L.; Tan, C. H.; Hu, S. M.; Wen, Y. H.; Wang, Y.; Fu, R. B.; Wu, X. T. *CrystEngComm* **2013**, *15*, 8139−8145. (c) Sun, C. Y.; Wang, X. L.; Qin, C.; Jin, J. L.; Su, Z. M.; Huang, P.; Shao, K. Z. *Chem.—Eur. J.* **2013**, *19*, 3639−3645.
(20) (a) Wang, D.; He, H.; Chen, X.; Feng, S.; Niu, Y.; Sun, D. *CrystEngComm* **2010**, *12*, 1041−1043. (b) Carlucci, L.; Ciani, G.; Maggini, S.; Proserpio, D. M.; Visconti, M. *Chem.—Eur. J.* **2010**, *16*, 12328−12341.
(21) (a) Zhang, Q.; Shreeve, J. M. *Angew. Chem., Int. Ed.* **2014**, *53*, 2540−2542. (b) Kumar, A. S.; Ghuyle, V. D.; Sahoo, A. K. *Chem.—Eur. J.* **2013**, *19*, 509−518.
(22) (a) Li, X. P.; Zhang, J. Y.; Pan, M.; Zheng, S. R.; Liu, Y.; Su, C. Y. *Inorg. Chem.* **2007**, *46*, 4617−4625. (b) Jin, X. H.; Sun, J. K.; Cai, L. X.; Zhang, J. *Chem. Commun.* **2011**, *47*, 2667−2669.
(23) Fei, H. H.; Bresler, M. R.; Oliver, S. R. J. *J. Am. Chem. Soc.* **2011**, *133*, 11110−11113.
(24) Stuart, B. *Infrared Spectroscopy: Fundamentals and Applications*; John Wiley & Sons, Ltd: Chichester, U.K., 2004; p 102.
(25) Shi, P. F.; Zhao, B.; Xiong, G.; Hou, Y. L.; Cheng, P. *Chem. Commun.* **2012**, *48*, 8231−8233.